General Disclaimer

One or more of the Following Statements may affect this Document

- This document has been reproduced from the best copy furnished by the organizational source. It is being released in the interest of making available as much information as possible.

- This document may contain data, which exceeds the sheet parameters. It was furnished in this condition by the organizational source and is the best copy available.

- This document may contain tone-on-tone or color graphs, charts and/or pictures, which have been reproduced in black and white.

- This document is paginated as submitted by the original source.

- Portions of this document are not fully legible due to the historical nature of some of the material. However, it is the best reproduction available from the original submission.

FINAL REPORT

NASA CR-
147508

Contract NAS 9-12563

National Aeronautics and Space Administration
Johnson Spacecraft Center

Houston, Texas

GRAVITY AND CRUSTAL STRUCTURE

by

Carl O. Bowin

Woods Hole Oceanographic Institution

February 20, 1976

TABLE OF CONTENTS

INTRODUCTION

To the Principal Investigator this has been a most satisfying contract to have been involved in. The challenge of studying a remote planetary body, of using new data types, of developing new analysis procedures has been stimulating and fruitful. At the onset of this contract four years ago the Principal Investigator felt that his experience studying earth features would be useful for interpreting lunar data, and that the broadening of one's vista would, in turn, be helpful for understanding our home planet, the earth. It is gratifying to find that these assumptions have proved true. It is also gratifying to find at the conclusion of the contract that nearly all the efforts proposed have been successfully accomplished.

ACKNOWLEDGEMENTS

I would like to take this opportunity to express my thanks to Nat Hardy and Joe Dixon of the JSC TN3/Apollo Photo Data Analysis Task Manager Office for encouragement, assistance, and support throughout this effort. I am much indebted to W. R. Wollenhaupt of the JSC Mission Planning and Analysis Division for completing the development of the Extended Sequential Estimation Orbital computer program which provides estimates of the acceleration components of the space craft from Dopplar tracking data, for

providing lunar gravity data processed by this program, and for helping to explain to a novice the intricacies of orbital analysis. I thank William Sjogren of the Jet Propulsion Laboratory for many discussions and for providing preprints and data in advance of publication. And, at the Woods Hole Oceanographic Institution, Bruce Simon, Leon Gove, Carolyn Dean, Nan Galbraith, and Christine Wooding have contributed importantly to the success of this contract. Interactions with Wilfred Bryan and Peter Jezek working under NAS 9-12564 have also been very beneficial.

STATUS OF CONTRACT COMMITMENTS

The status of the principal stages for the investigation are summarized below following the underlined stage descriptions from the original contract document.

(1) Make gravity attraction calculations at a nominal altitude for simple 3-D geometrics to simulate craters and maria for initial evaluation of effects of topography.

a. Flat-moon models
b. Curved-moon models

A selection of the results from such simple models have been published as Figure 1 in Bowin, et al. (1975). These models have proved very useful, for they rather quickly showed that mare fill could not match the observed gravity measurements unless it is unreasonably thick.

(2) Attempt to develop a three-dimensional curved surface gravity attraction model program.

A three-dimensional curved surface gravity attraction model program has been successfully developed. It is very fast computationally and adds negligable computer time to that of a flat-surface 3-D program. Our program computes both the flat surface and curved surface solutions and outputs both values for study. The methodology for this program is given in the Appendix of the paper by Bowin, et al. (1975).

(3) Evaluate requirements for processing individual models taking into account curvature of lunar surface.

This evaluation was incorporated into the development of the curved surface 3-D gravity computer program, and a discussion of some aspects of this matter are discussed in the first three paragraphs on page 4949 of Bowin, et al. (1975).

(4) Make gravity attraction calculations as in (1), but for different altitudes.

a. Flat-moon models
b. Curved-moon models

Evaluate expected vertical gradients to be expected from various sized craters and maria.

Figure 1 of Bowin, et al. (1975) presents gravity anomalies computed at both 20 km and 100 km heights above the moon's surface, and Figure 4 in the same paper gives computed anomalies at all elevations between the surface and 300 km height. Consideration of the vertical gradients observed and from simple computed models helped lead me to the development of the two-body solution for mascon anomalies published by Bowin, et al. (1975).

(5) Compare vertical gravity gradients produced by homogeneous spherical shell lunar mass models with those from model studies in (4).

Included in discussion of (4) above.

(6) Determine anomalous vertical gradients from comparison of gravity anomalies obtained at the same latitude and longitude but at different altitudes from the Orbiter and Apollo missions.

We attempted this, but the rev to rev variations from the sequential estimation Apollo radial component data were such that this effort was set aside. The low altitude sequential estimation Apollo data and the line-of-sight Apollo data were received too late in the contract period to be incorporated.

(7) Determine best approach for altitude reduction of spacecraft gravity data.

The best approach to date is to subtract a modeled acceleration at the position of the spacecraft from the observed acceleration of the spacecraft and take the difference to be the "free-air" gravity anomaly at the height of the measurement. The large variations in vertical gradient over mascon features would introduce considerable distortion of the anomalies if a standard vertical gradient were applied to all data from many different heights.

(8) Prepare (in conjunction with W. Sjogren and MSC) gravity anomaly map of moon's nearside with vertical acceleration values reduced to a common datum.

The difficulties discussed briefly in (7), the limited spacial distribution of the Apollo data, and the calculation of global gravity anomaly maps from orbital rate information by Ferrari (1975) lead to the defferement of this effort.

(9) Catagorize gravity anomalies with various crater and maria paramters.

Discussed in Bowin (1975).

(10) Select specific lunar features for detailed three-dimensional modeling.

Our analyses concentrated on the Serenitatis mascon

because it shows evidence of a large mascon, the Apollo 15 and 17 missions passed nearly over the center of the basin, and its simple, approximately circular outline is well defined by the surrounding highlands.

(11) Construct detailed surface and sub-surface three-dimensional models utilizing all geological and geophysical data available. To be done in conjunction with geologic studies by W. Bryan. Compare calculated gravity anomalies with those observed, and adjust models in accordance with geologic interpretation and gravity differences. This is an iterative, largely empirical, process by which limits of likely sub-surface mass variations are determined.

These procedures have led to the development of the two-body solution for mascon anomalies. This solution appears to be the geological most reasonable explanation for the magnitude of the mascon gravity anomalies.

(12) Interpret results in terms of crustal structure and origin of various crater and maria features on the moon.

Three papers dealing with such interpretations have been prepared under this contract. They are Bowin et al. (1975), Bowin (1975), and Bowin (1976). Copies of these papers are included in this report.

(13) Comparison and interpretation of the similarities and differences of the gravity fields of the earth, moon and Mars.

A paper (Bowin, 1976) with essentially this title has been submitted for presentation at the VII Lunar Science Conference scheduled for March 1976 in Houston, Texas. This analysis further suggests an explanation for the asteroid belt.

References Cited

Bowin, C. O., 1975. Negative gravity anomalies on the moon, Proc. of the Sixth Lunar Science Conference.

Bowin, C. O., 1976. Comparison of Gravity Anomalies for Earth, Mars, and Moon.

Bowin, C. O., Bruce Simon and W. R. Wollenhaupt, 1975. Mascons: A Two-Body Solution, Journal of Geophysical Research, Vol. 80, No. 35, pp. 4947-4955.

Ferrari, A. J., 1975. Lunar Gravity: The First Farside Map, Science, Vol. 188, pp. 1297-1300 (27 June 1975).

DATA FILES

We have prepared a digital data library on magnetic tape of single station extended sequential estimation gravity data from data received from Johnson Spacecraft Center for Apollo missions 14, 15, 16 and 17. These data are tabulated in Tables 1 and 2, and the format is described in Figure 1.

PUBLICATIONS

Three papers have been prepared under support from this contract. They are entitled, MASCONS: A TWO-BODY SOLUTION; NEGATIVE GRAVITY, ANOMALIES ON THE MOON; and COMPARISON OF GRAVITY ANOMALIES FOR EARTH, MARS, AND MOON. The last paper is being expanded for submission to a standard journal. Reproductions of the three publications follow.

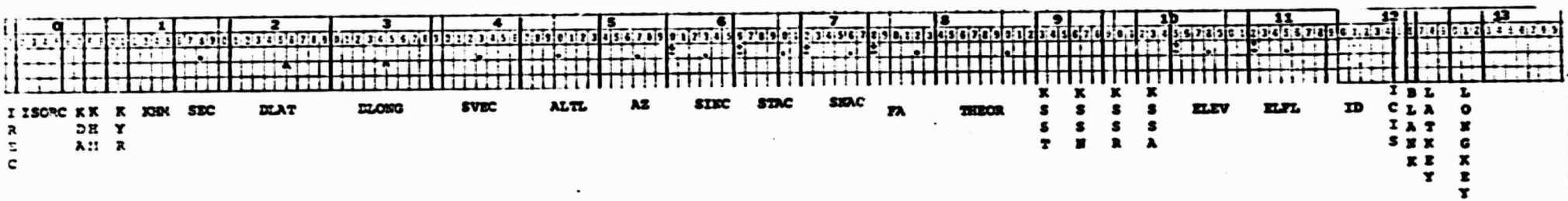

IREC - Indicator (=1 for present lunar data)
ISORC - W.H.O.I. Source Code
KDA - Day
KMO - Month
KYR - Year
KHM - Hour and minute
SEC - Seconds
DLAT - Latitude in degrees (+200)
DLONG - Longitude in degrees (+200)
SVEC - Vehicle distance from center of mass (KMS)
ALTL - Lasar altitude (kms)
AZ - Azimuth (degrees)
SINC - Inclination (degrees)
STAC - Tangential acceleration (mgals)
SNAC - Normal acceleration (mgals)
FA - Radial acceleration (mgals)
THEOR - Theoretical gravity (mgals)
KSST - Standard deviation of STAC (*100)
KSSN - Standard deviation of SNAC (*100)
KSSR - Standard deviation of FA (*100)
KSSA - Standard deviation of THEOR (*100)
ELEV - Elevation of topography w/ref to radius of 1738 KMS
ELFL - Lasar elevation of topography w/ref to radius of 1738 KMS
ID - Flight and Rev identifier
ICIS - Vehicle identifier
LATKEY - Sort key of latitude
LONGKEY - Sort key of longitude

. . decimal point ^ implied decimal point

Figure 1. Woods Hole Oceanographic Institution Lunar Gravity Format

TABLE 1.

Single Station Extended Sequential
Estimation Orbital Solutions

APOLLO 14

REV	Number of Data Points	WHOI Source Code	Tape Serial Number	File Number
1	496	163	GK14	1
4	384	163	GK14	2
7	385	163	GK14	3
10	296	163	GK14	4
13	382	163	GK14	5
17	339	163	GK14	6
23	421	163	GK14	7
29	407	163	GK14	8
34	387	163	GK14	9

TABLE 1.
(Continued)

APOLLO 15

REV	Number of Data Points	WHOI Source Code	Tape Serial Number	File Number
1	477	158	GK15	1
13	328	158	GK15	2
16	422	158	GK15	3
19	399	158	GK15	4
22	390	146	GK15	5
25	422	146	GK15	6
27	414	146	GK15	7
31	377	146	GK15	8
34	398	146	GK15	9
37	344	146	GK15	10
40	309	146	GK15	11
43	366	146	GK15	12
44	284	146	GK15	13
54	362	146	GK15	14
56	334	146	GK15	15
59	343	146	GK15	16
62	379	146	GK15	17
65	299	146	GK15	18
68	295	146	GK15	19
70	348	146	GK15	20
71	318	146	GK15	21
72	371	146	GK15	22

TABLE 1.
(Continued)

APOLLO 16

REV	Number of Data Points	WHOI Source Code	Tape Serial Number	File Number
1	480	160	GK16	1
3	354	163	GK16	2
6	368	163	GK16	3
9	365	163	GK16	4
12	346	163	GK16	5
17	429	160	GK16	6
22	329	160	GK16	7
27	425	160	GK16	8
32	395	160	GK16	9
37	213	160	GK16	10
42	399	160	GK16	11
47	431	160	GK16	12
52	430	160	GK16	13
57	400	160	GK16	14
61	422	160	GK16	15

TABLE 1.
(Continued)

APOLLO 17

REV	Number of Data Points	WHOI Source Code	Tape Serial Number	File Number
1	412	158	GK17	1
3	379	165	GK17	2
5	384	165	GK17	3
6	389	165	GK17	4
7	383	165	GK17	5
8	375	165	GK17	6
9	384	165	GK17	7
13	396	159	GK17	8
14	220	143	GK17	9
15	434	143	GK17	10
21	200	160	GK17	11
23	216	158	GK17	12
24	249	143	GK17	13
27	448	143	GK17	14
28	555	143	GK17	15
33	200	158	GK17	16
38	539	143	GK17	17
42	392	158	GK17	18
47	210	159	GK17	19
49	310	143	GK17	20
51	395	160	GK17	21
59	415	158	GK17	22
62	523	143	GK17	23
64	441	158	GK17	24
65	380	143	GK17	25
66	475	143	GK17	26
71	602	143	GK17	27
73	443	158	GK17	28
74	492	143	GK17	29

TABLE 2.

Single Station Solutions With
Laser Altitude

APOLLO MISSION	REV	Number of Data Points	Number of Data Points with Laser Altitude	WHOI Serial Number	File Number
15	16	422	121	GK15	3
15	22	390	227	GK15	5
16	17	429	51	GK16	6
16	37	213	54	GK16	10
16	47	431	118	GK16	12
17	14	220	61	GK17	9
17	15	434	118	GK17	10
17	24	249	75	GK17	13
17	27	448	79	GK17	14
17	28	555	161	GK17	15
17	38	539	160	GK17	17
17	49	310	107	GK17	20
17	62	523	147	GK17	23
17	65	380	44	GK17	25
17	66	475	106	GK17	26
17	71	602	193	GK17	27
17	74	492	119	GK17	29

VOL. 80, NO. 35 JOURNAL OF GEOPHYSICAL RESEARCH DECEMBER 10, 1975

Mascons: A Two-Body Solution

CARL BOWIN AND BRUCE SIMON

Woods Hole Oceanographic Institution, Woods Hole, Massachusetts 02543

W. R. WOLLENHAUPT

NASA Johnson Space Center, Houston, Texas 77085

Almost all of the mass distributions that have been proposed to account for the large positive gravity anomalies associated with lunar mascons have assumed single-body sources of a mass excess. In the case of mare fill with a reasonable density contrast (+0.5 g/cm³) with crustal material, a fill thickness of about 16 km for Mare Serenitatis is thus required to account for the observed gravity values at 100-km height. Such a great thickness would require a 16-km-deep hole prior to filling, and such a topographic depression is inconsistent with the depths of the topography of the Mare Nectaris and Mare Oriental basins, which have little fill, and with estimates of mare thicknesses based on buried crater dimensions. A two-body mascon solution, however, requires only about a 2-km thickness of fill and a 12-km rise of a lunar Moho beneath Mare Serenitatis to account for observed gravity anomalies. The mantle dome results from an uprising of mantle material beneath the mare basin, bringing the impact crater to near isostatic equilibrium. Two kilometers of fill is inferred to have accumulated later, when the crust became rigid enough to sustain the load. Together the fill and the dome account (at about 20% and 80%, respectively) for the magnitude of the observed mascon anomalies. This type of two-body solution can account for greater magnitude mascon gravity anomalies by proportional increases in the fill thickness. The top of the mantle dome or plug is placed at 60-km depth to match observed seismic velocity structure. This mascon structure has an anomalous gravity field that is in agreement with the maximum magnitude of anomalies observed at several heights above Mare Serenitatis. The thickness of fill would be greater if the basin floor had subsided under the load of early fill material.

INTRODUCTION

The origin of mascons (lunar mass concentrations) has been of interest since their discovery by *Muller and Sjogren* [1968]. Almost all of the mass distributions that have been proposed to account for the large positive gravity anomalies associated with mascons have been isostatically uncompensated structures. Examples of such structures are buried iron meteorites [*Stipe*, 1968], the pooling of a melt from an impacted meteorite [*Urey*, 1968], a mantle plug [*Wise and Yates*, 1970], or the mare fill itself [*Conel and Holstrom*, 1968; *Baldwin*, 1968; *Phillips et al.*, 1972; *Wood*, 1970; *Booker et al.*, 1970].

These models have all been single-body sources of a mass excess to account for the mascon gravity anomaly. *Phillips et al.* [1972, p. 7113] briefly discussed the possibility of a two-body mass anomaly consisting of both mare fill and a mantle plug. However, they did not consider that a plug would contribute significantly to the gravity effect observed. *Arkani-Hamed* [1973] proposed development of a 20-km-high mantle plug beneath Mare Imbrium immediately following impact, and he examined temperature variations with depth for such a structure. The gravitational attraction of this structure was not calculated.

Only *Hulme* [1972] has computed the gravitational attraction of a two-body mass anomaly distribution, and it is unique in being the only mascon structure so far proposed that could be in isostatic equilibrium (Figure 1*f*). The specific structure that he presents, however, is not in perfect isostatic equilibrium (W. L. Sjogren, personal communication, 1974), because the crustal layer is thinner beneath the center of the mare and thicker at the margin than is required for equilibrium.

Wise and Yates [1970] proposed that a mantle plug formed following the formation of a deep crater by meteorite impact. The rise of this plug and the concomitant volcanic fill reestablished isostatic equilibrium but still left a crater some 6.4 km deep. Because a quantity of volcanic material is less dense when it is molten than when it is solid, Wise and Yates postulate that continued flooding of the crater by lava occurred until the excess of lithostatic pressure over hydrostatic pressure could lift the magma no further. The continued flooding produced a superisostatic fill. In their analysis Wise and Yates inferred that the volcanic fill has the same density as the normal lunar crust, and hence they concluded that after the mare basin filled with this material, '. . . the fill would disappear gravimetrically, and the residual positive anomalies in the gravity picture would be due to the Moho plug plus any topographic effects.' This is the case because in their model the density of the superisostatic fill is the same as the density of the surrounding crust. By assuming a density contrast of 0.5 g/cm³ between the plug and the lunar crust the gravitational attraction of several configurations for the mantle plug was computed to match the Lunar Orbiter data for Mare Imbrium [*Muller and Sjogren*, 1969]. For the model assuming a crustal thickness of 61 km the height of the mantle plug is 31 km, and the depth to the top of the plug is 30 km.

In this paper we present theoretical free-air gravity anomalies that occur over a variety of simple structural configurations for reference and as an aid to the understanding of the constraints imposed by the observational gravity data. These calculations take into account the curvature of the lunar surface. The computer program which performs these computations is described in the appendix. By means of the simple structures presented, available observational gravity data, and information on the depth of mare fill and rock densities we argue that a single-body mass anomaly is not adequate to explain the mascon gravity anomalies, and we present a preferred two-body solution.

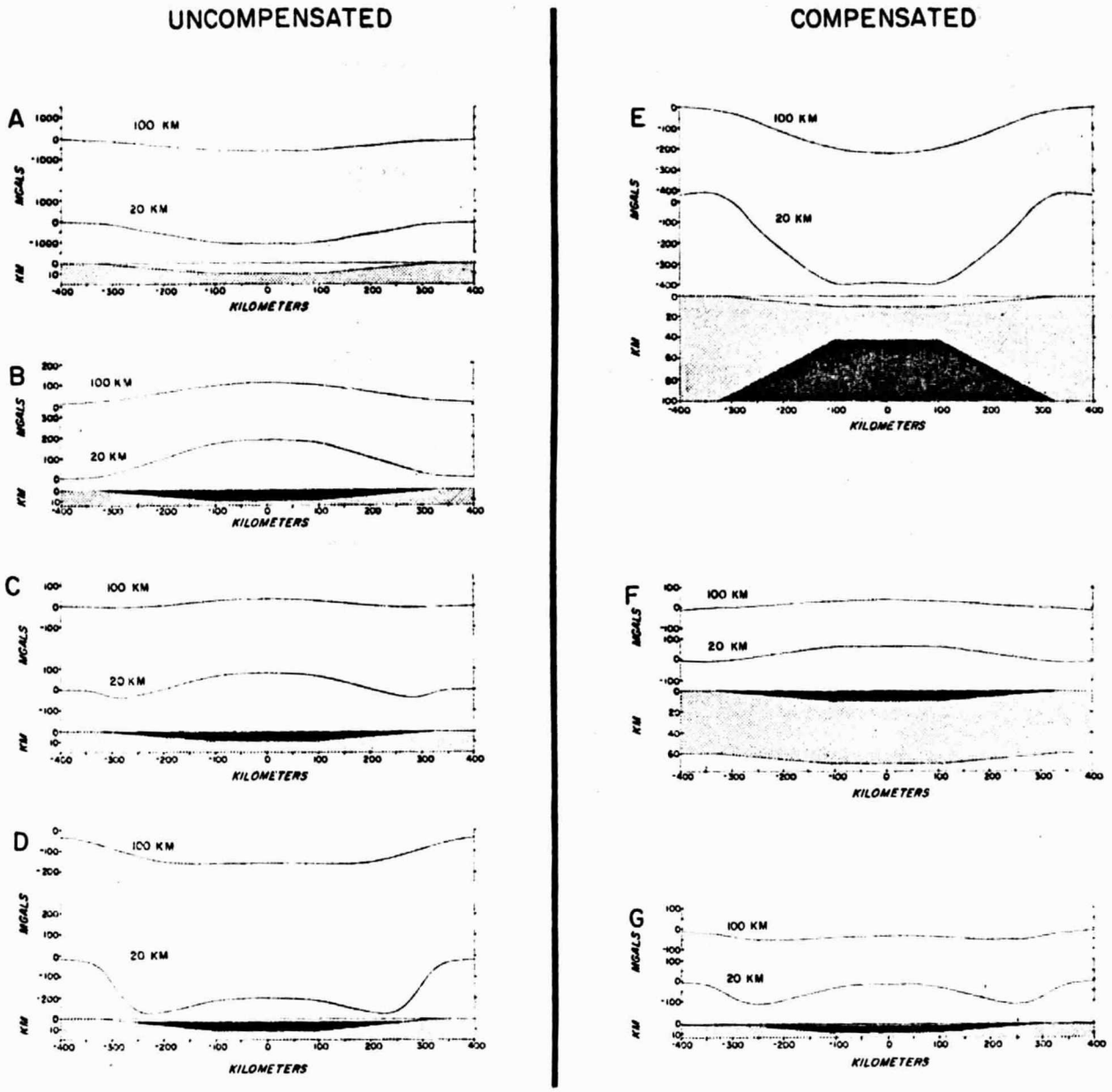

Fig. 1. Cross sections of mare basin structures and their gravity anomalies. Structures on the right are in isostatic equilibrium, and those on the left are not. Lunar crust is indicated by stippled pattern (assumed density of 2.9 g/cm³). Mare fill and source of mascon anomaly are indicated in black (assumed density of 3.4 g/cm³). The unfilled mare basin (density of zero) is left unpatterned, as is the lunar mantle (density 3.4 g/cm³) in part *f*. In parts *g*, *c*, and *d* the thickness of the fill is 8.53 km, and the overlying depressions are 1.47, 0.67, and 2.97 km deep, respectively.

SIMPLE MARE MODELS

The free-air anomalies that would be associated with several simple mare basin configurations are shown in Figure 1. The configurations in the right-hand column are isostatically compensated, and those in the left-hand column are not. The free-air anomaly profiles are not diagrammatic but are accurately calculated from the models by taking into account the curvature of the moon by means of the computer program described in the appendix. Free-air anomaly profiles (Figure 1) are given at both 20- and 100-km height in order to give the reader a better feeling for the change of the anomaly magnitude with height.

A hypothetical sequence of mare evolution follows to illustrate changes in the gravity field that would occur over a 10-km-deep basin. This hypothetical sequence does not involve any deep anomalous mass distributions; it involves only those of the basin and its fill. Prior to the filling of the basin (Figure 1*a*), large negative gravity anomalies would occur. As the basin began to fill, the magnitude of the negative anomaly would decrease, and a local gravity high would develop in the center (as occurs in Figure 1*d* but with much less than 10 km of fill). At a certain stage of filling (Figure 1*g*) the thickness of the fill would be such that its mass in excess of that of the equivalent volume of crust would just equal the mass deficiency of the remaining void above the fill, and the structure would be in isostatic equilibrium. Additional filling would lead to an excess of mass and to positive gravity anomalies (Figure 1*c*). Upon complete filling of the basin (Figure 1*b*) the greatest positive anomaly would occur. We might now imagine that

the basin floor would begin to sink. This would lead to a reduction in the magnitude of the positive gravity anomaly (Figure 1*c*). Sinking might continue until isostatic equilibrium again occurred (Figure 1*g*). If sinking continued further, negative gravity anomalies would become more and more pronounced (Figure 1*d*). Of course, all these stages need not be imagined, and some intermediate stages might be bypassed in other hypothetical sequences. The models of Figure 1 are illustrative of the free-air anomalies that would be expected for a variety of possible evolutionary paths.

For the calculation of gravity anomalies for the models of Figure 1 there are two general approaches. One can use the actual assumed densities of each of the portions of the model, sum their attractions, obtain the difference between the total attraction and the known or assumed anomaly value at some location, and add that difference algebraically to the total attraction value at other locations to obtain anomalies. Or one can assign only the value of density contrasts to each portion of the model. The two methods provide identical results except in the case in which the strong gravity gradients that occur at the truncated edges of the model also have an appreciable effect on the portion of interest in the model. This condition is the case for three-dimensional models of circular maria on the moon's surface. Accordingly, better results are obtained if density contrasts are used in the computations. The density contrasts are those mass distributions that differ from the mass distribution of a moon composed of homogeneous concentric spherical shells.

For all the gravity calculations for all the models of Figure 1 the gravitational attraction of the mare fill is only that of the density contrast between the fill and the crust material. For the whole rock density to be used as a density contrast in computing its gravitational attraction the fill would have to be isolated laterally from the surrounding crust. That is, it would have to be above the normal level of the lunar crust. This type of model is not shown in Figure 1 because the mascon anomalies occur over depressions, rather than highs, in the lunar topography.

In this paper we assume that the normal level of the lunar crust is equal to that of the mare surface. This, of course, may not be true. The mare surfaces may have sunk, or the mare depression may not have been filled as high as the normal level of the lunar crust. If the latter situation is assumed, then a volume of space having a density of zero (or a contrast of minus the lunar crust density) should be incorporated into a model used for gravity computations. Zero density leads to very large mass deficiencies, as is readily clear from the large negative free-air anomaly of Figure 1*a*. Thus to produce the mascon anomaly, the subterranean mass excess must be greater than the value obtained if the normal level is taken at the mare surface. Because the observed gravity anomalies (Figure 2*a*) do not indicate the occurrence of large positive values over the highlands, we assume that the mass of the topographic elevation of the highlands above the mare surface generally is largely compensated at depth by a mass deficiency. This is probably due to a thicker crust, which for the purposes of this paper has not been included in the structure models.

LUNAR GRAVITY DATA

Mascons were discovered by *Muller and Sjogren* [1968] during their processing of Lunar Orbiter tracking data. Several recent studies of lunar mascons have concentrated on an analysis of the gravity field over Mare Serenitatis [*Conel and Holstrom*, 1968; *Hulme*, 1972; *Sjogren et al.*, 1972; *Phillips et al.*, 1972]. Serenitatis is of interest for several reasons. It shows evidence of a large mascon, the Apollo 15 and 17 missions passed nearly over the center of the basin, and its simple, approximately circular outline is well defined by the surrounding highlands.

Muller et al. [1974] determined a maximum free-air anomaly value of +230 mGal at a height of 15 km over Mare Serenitatis. This anomaly was based on performing spline fits to the converged least squares Doppler residuals in determining line-of-sight acceleration [*Sjogren et al.*, 1974]. At the longitude of Serenitatis the line-of-sight acceleration should be only about 5.5% lower than the moon's radial component of gravity acceleration.

The gravity data for this analysis were obtained with a relatively new computer program developed at the Johnson Space Center. This program uses extended sequential estimation techniques for processing the Doppler data to solve for the spacecraft state vector. During computation the spacecraft state vector and the components of the unmodeled accelerations are simultaneously determined. The spacecraft state vector consists of the components of the position and velocity vector of the spacecraft at each data measurement time. Doppler residuals are obtained by subtracting from the observed Doppler signal a modeled acceleration based on a gravity model known as the L1 model. This model contains the following spherical harmonic coefficients: $J_{20} = 2.07108 \times 10^{-4}$, $C_{22} = 0.20716 \times 10^{-4}$, $J_{30} = -0.21 \times 10^{-4}$, $C_{31} = 0.34 \times 10^{-4}$, and $C_{32} = 0.02583 \times 10^{-4}$. The unmodeled accelerations are determined for three components: radial (toward the center of the moon), tangential (in the direction of the orbit path and normal to the radial component), and normal (perpendicular to the orbit path and at right angles to the other two components). The radial acceleration is equivalent to free-air anomalies at the elevation of the observations.

The resolution of the program is primarily limited by the noise on the tracking data. The major source of this noise appears to be short-term differences between the cesium frequency standards at the individual tracking stations. When one is simultaneously processing multiple-station data, the noise in the estimated accelerations is of the order of 15–20 mGal (Figure 2*b*). If data from only one tracking station are processed, the noise appears to be of the order of 5 mGal (Figure 2*a*). The revolution to revolution consistency is normally within about 5 mGal. Occasionally, the difference is up to 20 mGal. The loss of parallax information in the single-station solutions results in attenuation of the estimated or recovered accelerations. This is particularly true for the limb regions, say, >60° longitude. For Serenitatis the attenuation was only about 15 mGal. Since this article is primarily concerned with the central region, it was decided to use the single-station solutions. It is estimated that the recovered accelerations in this region, derived from single-station solutions, are good to 40–60 mGal for the individual components and to about 20–30 mGal for the total recovered acceleration. The unmodeled radial accelerations estimated by this program are consistent with the Jet Propulsion Laboratory (JPL) line-of-sight accelerations within the limitations of each technical approach.

Large negative free-air anomalies are observed in the Apollo Command Ship Module (CSM) tracking data adjacent to the positive anomalies associated with mascons. The negative anomaly is especially pronounced between Mare Crisium and Mare Serenitatis. The origin of these lows is not known. They appear to be real features and not artifacts of the processing

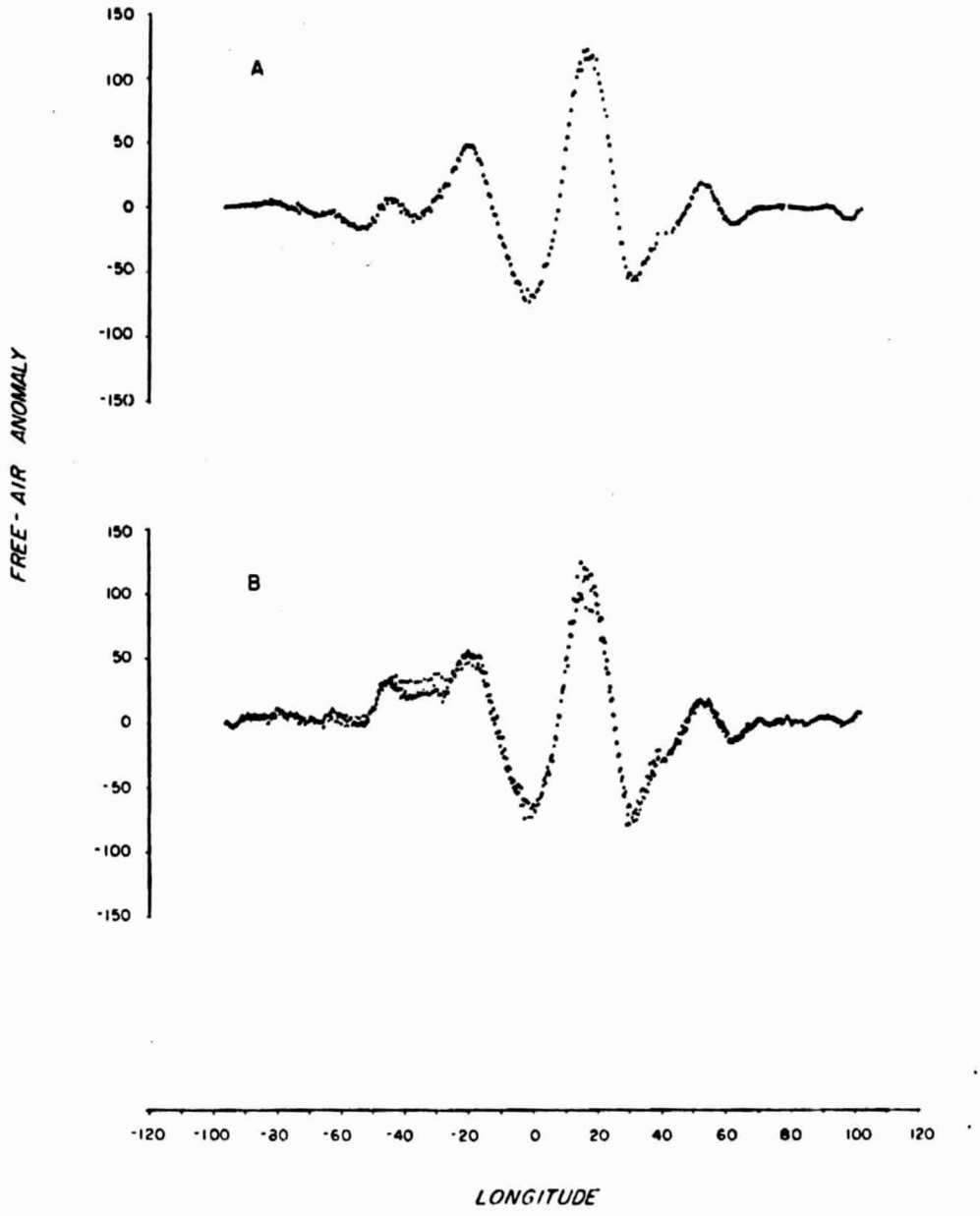

Fig. 2. Free-air gravity anomalies from Apollo 15 revolution 31. (*a*) Single-tracking station solution. (*b*) Multiple-tracking station solution.

techniques, because a large negative free-air anomaly (-213 ± 8 mGal) was derived [*Sjogren et al.*, 1974] at the Apollo 17 landing site from the Lunar Traverse Gravimeter results [*Talwani et al.*, 1973] and it coincides in location with the negative anomaly minimum found in the orbit tracking data (Figure 3).

The negative gravity anomalies adjacent to mascons have commonly been inferred to ring the mascon completely [*Wise and Yates*, 1970; *Hulme*, 1972; *Arkani-Hamed*, 1973]. This assumption does not appear to be generally true. Figure 3 shows the location of free-air anomaly minima on the sides of Mare Serenitatis as observed in the Apollo 15 revolution having a height of more than 100 km. This figure is based on single-station solutions, for which the crest and trough of anomalies are more sharply defined than those for multiple-station solutions. These data clearly show that the free-air minimum on the east side of Serenitatis does not continue around to the southern margin of the mare. Also, the positive anomaly of the Serenitatis mascon extends beyond the southern margin of the mare (although it is much diminished in magnitude there) at least as far as the distance from the trough of the minimum to the east margin. A map of line-of-sight accelerations over Mare Serenitatis and the region to the south and east prepared by W. L. Sjogren (personal communication, 1975) from Apollo 15 CSM data for revolutions 15–70 is consistent with the above interpretation.

MARE FILL THICKNESS AND DENSITY CONTRAST

Gravity anomalies result from a distribution of mass anomalies and hence depend upon the volume, density, and location of the mass anomalies. Thus from gravity data alone it is impossible to define uniquely the thickness of the mare fill and its density contrast with the crustal material. That is why the inverse solutions presented by *Phillips et al.* [1972, Figures 2 and 4] are given in terms of surface densities for various depths. For zero depth a surface density of about 8 (g/cm^3) km

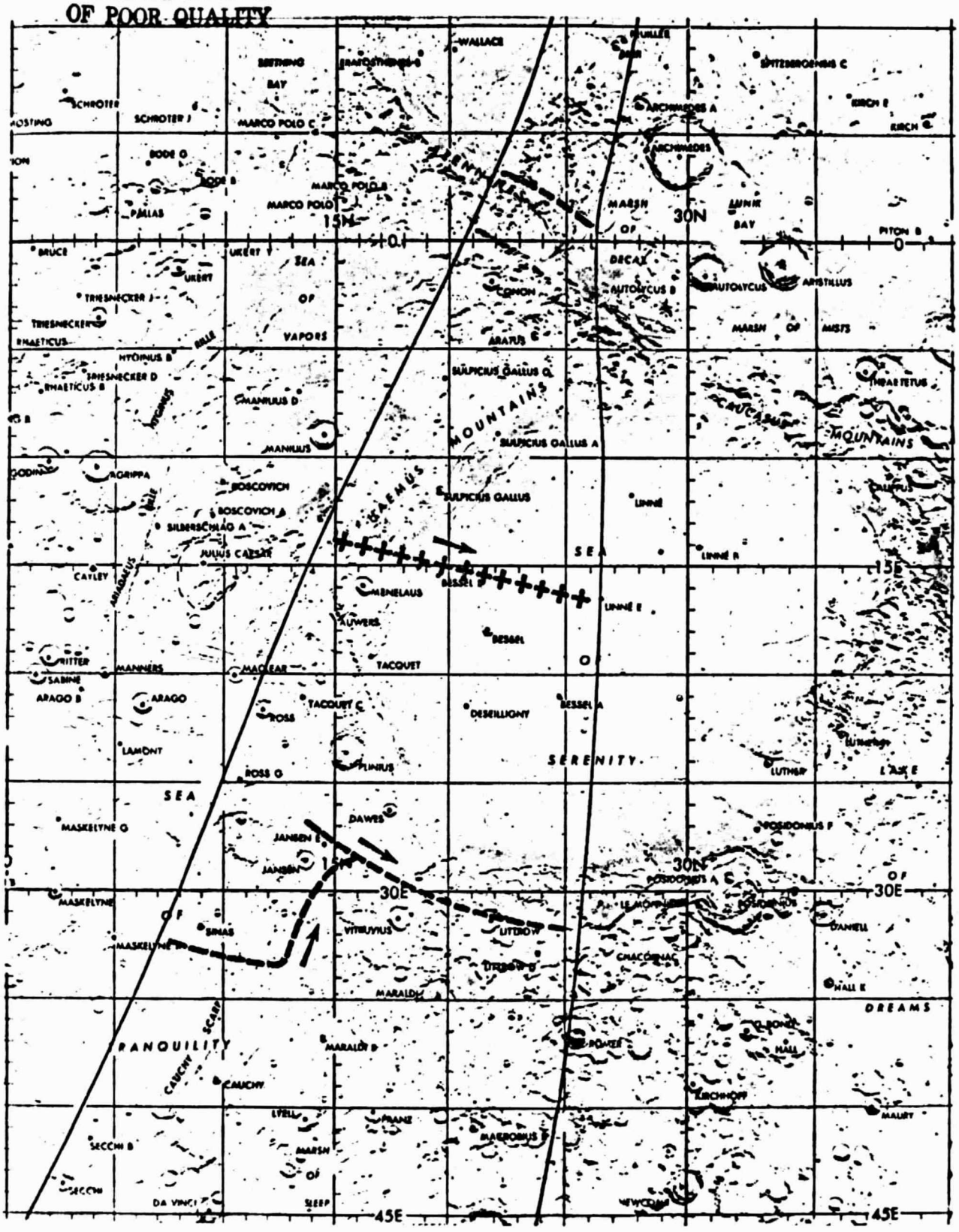

Fig. 3. Location of free-air anomaly minima and maximum in Mare Serenitatis region. Minima are indicated by dashes, and maximum by pluses. Data boundaries from those Apollo 15 orbit revolutions 1-72 having more than 100-km height are shown by thin solid lines.

was determined for the Serenitatis mascon. This value corresponds, for example, to a fill thickness of 8 km for a density contrast of 1.0 g/cm³ or to a thickness of 16 km for a density contrast of 0.5 g/cm³.

Conel and Holstrom [1968] matched the peak-to-trough amplitude (from about +170 to −80 mGal) for the Serenitatis mascon and determined a fill thickness of 14 km for a density contrast of 1.1 g/cm³. They recognize that this is an unusually

high density contrast to accept. They also determined a fill thickness of 30.8 km for a density contrast of 0.5 g/cm³. Using an infinite slab approximation, *Wood* [1970] calculated that a 1-km-thick layer of density 3.3 g/cm³ would give rise to a gravity anomaly of about +140 mGal and hence would be comparable to mascon anomalies. As was discussed previously, the density contrast, not the rock density, must be used in such calculations. In addition, Wood's estimate of the gravitational anomaly is too high because it was based on the assumption that the 1-km-thick layer is an infinite slab. The gravitational attraction of an infinite slab is independent of the distance from the surface of the slab. Taking into account the finite dimensions of a 1-km-thick layer (of 3.3-g/cm³ density) of mare fill of 320-km radius, we calculate that a gravitational anomaly of 98 mGal at 100-km height would be produced, a reduction of 30% from the infinite slab approximation.

From the preceding review it is clear that the fill in a mare basin such as Serenitatis would have to be about 16 km thick if it had a density contrast of 0.5 g/cm³ with the normal crustal material in order to account for the mascon gravity anomaly. Such a great prefill basin topography seems highly unlikely. This thickness would be reduced to about 8 km if the density contrast were 1.0 g/cm³; however, such a high density contrast is unlikely.

Density measurements on lunar samples are unfortunately very limited. A summary of published and unpublished values is given by *Talwani et al.* [1973]. If one excludes those measurements for which the volume was determined from aluminum foil models, the densities of the basalt samples range from 2.8 to 3.4 g/cm³, and those of the breccia samples range from 2.2 to 3.0 g/cm³. The three basalt samples measured by hydrostatic weights all provide a density of 3.4 g/cm³. Those samples for which porosity was also determined indicate that intrinsic densities range from 3.25 to 3.49 g/cm³ for the three basalts and from 2.99 to 3.14 g/cm³ for the five breccias. Although near-surface rocks may have low bulk densities because of their vugs, vesicles, or fractures, within a few kilometers of depth they should nearly approach their intrinsic grain density. Thus for constructing structure models for gravity studies the assumption of a basalt density of 3.4 g/cm³ and a density contrast of 0.5 g/cm³ with highland breccia material (rock density of 2.9 g/cm³) is supported by the available measurements. The density contrast of 0.5 g/cm³ may be slightly high.

For a density contrast of 0.5 g/cm³, if the thickness of mare fill in Serenitatis is less than 16 km, the resulting maximum free-air anomaly over the mare will be less than that observed (Figure 1*b*). Since the maximum anomaly value for individual mascons appears to be proportional to the size of the mare basin, the last statement is probably true for the other mascons as well as for the one at Serenitatis.

Evidence from crater counts and from radioactive age dating of returned samples suggests that considerable time (perhaps about 200×10^6 years) elapsed between the formation of the large mare basins and their filling by mare basalts [*Baldwin*, 1963, 1971; *Huneke et al.*, 1973]. The existence of mascons appears to provide evidence that the rigidity of the lunar crust was increasing during the same interval [*Baldwin*, 1971; *Phillips et al.*, 1974; *Muehlberger*, 1974]. A 10-km-deep compensated hole in the lunar surface would have a free-air anomaly of about −385 mGal (Figure 1*e*), and a 16-km hole would have an even greater negative gravity anomaly. Since gravity anomalies that large are not observed on the moon and since the present lithosphere is considered to be more rigid now than when the mare basins were formed, the premare fill depression was probably only a few kilometers deep at most. This deduction is compatible with estimates of the thickness of mare fill in shelf regions on the basis of inferred dimensions of buried craters [*Marshall*, 1963; *Baldwin*, 1971; *De Hon*, 1974]. These results suggest thicknesses of mare fill that are less than 2 km. Probably less than 1 km of fill occurs in the shelf area of Mare Imbrium [*Baldwin*, 1971]. The average thickness within Mare Tranquillitatis is 500–600 m, with a maximum accumulation in excess of 1200 m in the vicinity of Lamont crater [*De Hon*, 1974]. The flooded inner basin of Nectaris has a fill that is at least 1.2 km thick. The maximum thickness is undetermined but may not exceed 1.5–1.6 km [*De Hon*, 1974]. Mare Nectaris and Mare Oriental have little fill in comparison with Crisium, Serenitatis, and Imbrium but do not show a pronounced increase in depth as the center of the basin is approached. From this comparison and from the estimates of fill thickness from buried craters it is very unlikely that great thicknesses of mare fill occur in the centers of the mare basins.

The small mascon gravity high over Tranquillitatis correlates in location with the thicker section of fill material at Lamont [*Phillips and Saunders*, 1974]. Again, however, the 1.2-km-thick section at Lamont can only yield the mascon gravity anomaly value if a high density contrast (of about 3.15 g/cm³) is assigned to it [*Phillips and Saunders*, 1974]. Such a density contrast is not realistic, and even though the prefill topography may have been in isostatic equilibrium, it would not be correct, as was explained previously, to use the rock density of the superisostatic fill in gravity model calculations. Hence the fill alone cannot explain the mascon gravity anomaly.

From the foregoing discussion it seems to be amply demonstrated that the mascon gravity anomalies are not produced simply by the occurrence of a superisostatic fill in mare basins. The fill alone is too thin to account for the large positive anomalies observed. It is also indicated that the mass distribution causing the mascon anomalies must be out of isostatic equilibrium.

TWO-BODY MASCON SOLUTION

A simple solution to account for the mascon anomaly can be achieved by considering the mass excess to occur in two bodies rather than in a single body. This solution conceptually is much like that of *Wise and Yates* [1970], except that here the fill, as well as the mantle plug or dome, is considered to contribute to the mascon anomaly. Consider the premare basin to have had a structure like that in Figure 1*e*, only not nearly so deep. This structure would be in isostatic equilibrium because a mantle dome having excess mass rose to balance the mass deficiency of the depression in the crust surface caused by a large impact. For the model of Figure 4, 14 km of crust is inferred to have been blasted away by the impact, an action resulting in a thinned crust. Note that although this structure is in isostatic equilibrium, the free-air anomaly would not be zero over the crater basin. Instead, negative values would occur at the center. The magnitude of the minimum depends considerably upon the thickness of the crust. As the mantle dome approaches the surface more closely, the magnitude of the minimum diminishes; if the dome lies at greater depths, the minimum increases. This is known as the topographic effect, which results because gravitational attraction varies inversely as the square of distance, and the deficiency of the crater is closer to the gravity observation site than is the excess of the mantle dome.

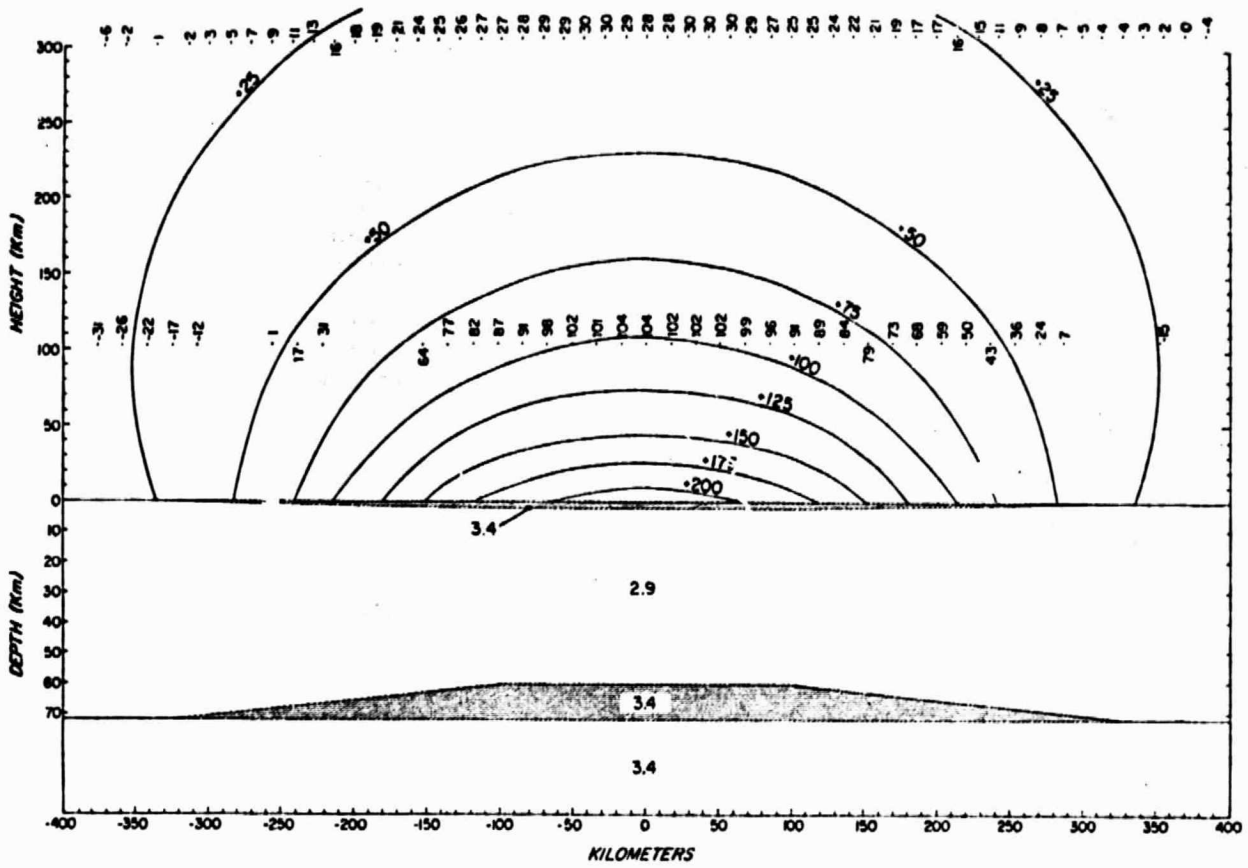

Fig. 4. Two-body mascon structure model. Figure shows a cross section through the center of a radially symmetrical three-dimensional structure. Isoanomaly lines show computed free-air anomalies above this structure. Numbers in the model are densities in grams per cubic centimeter. Shaded bodies are the mass excess producing the mascon gravity anomaly. Values in space are observed free-air anomalies from Apollo 15 revolutions 1 (higher) and 22 (lower).

It is likely that the rigidity of the lunar crust increased with time, following the formation of the mare basin. Thus at the time of the surface eruption of the mare fill volcanism the rigidity of the crust would be such that it could sustain the load due to the fill without the occurrence of major isostatic adjustments at depth. A structure model for Mare Serenitatis based on this evolutionary outline is shown in Figure 4. Prior to filling, the basin was 2 km deep in crustal material having a density of 2.9 g/cm³ and is inferred to have been isostatically compensated by a 12-km rise of lunar mantle material having a density of 3.4 g/cm³. This depression would have had a minimum free-air anomaly value of about −44 mGal over the center at 100-km height. During the interval 3.9–2.1 × 10^9 years ago, filling of this basin by flooding of basalt lava occurred [*Huneke et al.*, 1973]. Although there is evidence for some subsidence of Mare Serenitatis [*Bryan*, 1973; *Muehlberger*, 1974], the crust is assumed to have been sufficiently rigid to support the main load represented by this volcanic fill. The magnitude of the excess load is 680 kg/cm² beneath the center of the basin, when a lava density of 3.4 g/cm³ is assumed. However, its anomalous gravitational attraction results only from the density contrast of the fill with the surrounding crust (taken to be +0.5 g/cm³ in the model of Figure 4). Since the large mass deficiency that previously existed because of the unfilled depression has now disappeared, the gravitational attraction of the density contrast between the mantle plug and the adjacent crust is no longer canceled by the negative attraction of the topographic depression. Hence the plug's anomalous attraction adds to that of the fill, the combination resulting in a large positive gravity anomaly over the mare.

At a height of 17 km above the center of the model (Figure 4) the fill contributes 21.3% of the total anomalous gravitational attraction, and the mantle dome 78.7%. The percentage contribution of the fill diminishes gradually with increasing height, so that at 300 km it is 18.9% and that of the mantle dome is 81.1%. If a deeper (or shallower) original mare basin were assumed, then a greater (or lesser) total anomalous gravitational attraction would result from the model, but the percentage contributions of the mantle dome and fill would not change greatly. Differences in the assumed density contrasts could be accommodated within limits by different original mare basin depths and yet could have nearly the same total anomalous gravitational attraction for the models. The fill and the mantle dome could also be assumed to have different densities. As greater confidence in the precision and accuracy of the lunar gravity anomalies is obtained, it may become possible to limit more the relative contributions of shallow and deep sources for the mascon anomalies. Without the gravitational contribution of the fill the mantle dome alone would not match the observed values. To match the total anomaly of Figure 4 would require that the mantle have a density contrast with the crust of 0.63 g/cm³. But of course if it did, then it would be smaller in volume and hence would have less gravitational attraction, since the dome would not need to rise as high in order to provide compensation for the mass deficiency of the basin. It therefore seems most likely that both mantle

dome and fill contributions are required to explain mascon gravity anomalies.

In the model of Figure 4 the top of the mantle dome was located at 60-km depth to be compatible with the limited information available on the seismic velocity structure of the moon [*Lammlein et al.*, 1974]. No marked change in seismic compressional velocity is noted at the 1- to 3-km depth corresponding to the base of the mare fill. We have no explanation for this possible disagreement with our mascon model (Figure 4), except to suggest that perhaps the fractured nature of the shallow material may mask the velocity contrast that would be expected of the assumed density contrast.

The two-body mascon model shown (Figure 4) is in agreement with the large positive free-air gravity anomaly values determined from lunar-orbiting spacecraft. Single-station solution values for Apollo 15 revolutions 1 and 22 are given in Figure 4. The theoretical anomaly values are on a plane across the center of the circular symmetrical structure model. The observational data are plotted with respect to the maximum anomaly value along its particular orbit. Revolution 1 passed closer to the presumed center of the Mare Serenitatis mascon than did revolution 22. However, the data for these revolutions are considered to be representative and to indicate the general agreement between the two-body mascon solution and the observational data. Preliminary processing of low-altitude (about 20 km) revolutions for Apollo 15 (revolutions 3–12) indicates agreement with the theoretical values of the model (Figure 4). The agreement between the theoretical and the observational data diminishes toward the periphery of the mare basin because the model does not account for the large negative anomalies that flank the basin along the trajectories of the Apollo 15 and 17 missions.

The loading of this mascon structure model (Figure 4) is 680 kg/cm². This value is slightly less than the 800-kg/cm² loading value derived by *Sjogren et al.* [1972] for Mare Nectaris and by *Phillips et al.* [1972] for Mare Serenitatis. This lower value arises because the radial component derived from the sequential estimation program generally yields lower-magnitude anomalies than does the JPL spline fit program for the total acceleration. Increasing the fill thickness and the elevation of the mantle dome of our model (Figure 4) can make it compatible with higher mascon anomaly values. The percentage increase in fill thickness is approximately the same as the percentage increase in the anomaly. For example, a 150-mGal mascon anomaly at 100-km height would be produced by a fill thickness of 2.9 km.

In addition to possible errors in assuming rock densities or matching calculated anomalies to a gravity value that is too low, the fill may actually be greater than 2 km thick for another reason. If sinking of the basin floor occurred in the early stages of basin filling in response to loading due to the fill, then some portion or all of the early fill, depending upon the amount of sinking, would be compensated by the depression of the floor. During at least the later stages of mare filling the lunar crust became rigid enough to support the mass of the new fill without sinking. If all the filling occurred after this condition had been achieved, then only about 2 km of fill is required (together with the mantle dome) to account for the mascon gravity anomaly.

The structure model of Figure 4 provides a two-body mascon solution that can account for the gravity field so far observed at several heights over the central part of Mare Serenitatis. The thickness of the mare fill and the density values assumed are consistent with the data available.

APPENDIX: GRAVITATIONAL ATTRACTION FROM A THREE-DIMENSIONAL BODY ON A CURVED SURFACE

As the size of a body whose gravitational anomaly one wishes to compute becomes relatively large in comparison with the radius of curvature of the sphere in which it resides or if the anomaly is desired at points distant along the surface, it becomes necessary to employ equations which account for this curvature. Following the procedure of *Talwani and Ewing* [1960] the body is divided into polygonal contours, which are subdivided into triangular segments. As the attraction from each triangular lamina segment is exactly computed, a curved correction term is added to it, producing a net anomaly for a curved triangular lamina segment. This correction term is both accurate and quickly computable.

The vertical component of gravity from a curved triangular lamina segment is given in spherical coordinates by (see Figure 5*a*)

$$\Delta g = \Delta Z k \rho \iint \frac{\cos \alpha}{r^2}\, dA$$

$$= \Delta Z k \rho \iint \frac{R^2 \sin \theta\,(Z - R \cos \theta)}{r^3}\, d\theta\, d\phi$$

$$= \Delta Z k \rho \int_{\phi_1}^{\phi_2} \left[\frac{R^2}{Z^2} + \frac{rR}{2Z^2} - \frac{R(Z^2 - R^2)}{2Z^2 r}\right] d\phi \qquad (1)$$

where

- k universal gravity constant;
- ρ density;
- ΔZ thickness of polygon;
- R radius of body;
- r distance from field point to edge of laminae;
- Z_0 height of field point above surface, equal to $Z - R$;
- α angle to vertical;
- θ, ϕ spherical coordinates.

As $R \to \infty$,

$$\Delta g \to \Delta Z k \rho \int_{\phi_1}^{\phi_2} \left(1 - \frac{Z_0}{r}\right) d\phi \qquad (2)$$

the flat expression.

Our task, then, is to compute the integral in (1) along each edge of the polygon. Unfortunately, unlike the expression for a flat body [*Talwani and Ewing*, 1960], the expression for a curved body is not analytically integrable along an edge, nor is it easy to approximate by using series or other integration techniques. However, the integral of the difference between the flat and the curved integrands can be easily approximated along an edge, and this difference added to the exact flat expression results in a good approximation to the curved integral.

To do this, we will divide each lamina segment into four equally spaced regions (in ϕ) (see Figure 5*b*) and apply a parabolic approximation to the integral using the resulting five points. Let A_n be the distance from the nth point on the lamina to the vertical projection of the field point on the surface (see Figure 5*c*). Let the difference between the flat and the curved expressions be

$$D_n = 1 - \frac{Z_0}{r_n'} - \frac{R^2}{Z^2} + \frac{Rr_n}{2Z^2} - \frac{R(Z^2 - R^2)}{2Z^2 r_n} \qquad (3)$$

where $r_n' = (Z_0^2 + A_n^2)^{1/2}$ is the flat distance from the field point to the nth edge point and $r_n = [R^2 + Z^2 - 2RZ \cos (A_n/R)]^{1/2}$ is the corresponding curved distance. The integral

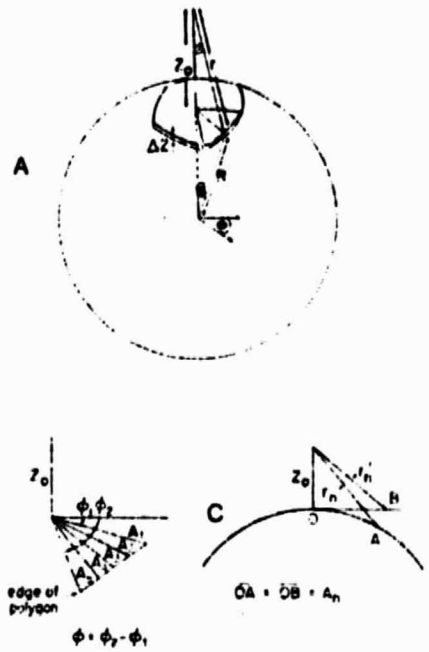

Fig. 5. Geometrical elements involved in calculating the vertical gravitation attraction of a spherical triangular cap.

of the difference is then given by a parabolic approximation for five equally spaced points:

$$C = (\phi/96)(9D_1 + 28D_2 + 22D_3 + 28D_4 + 9D_5) \quad (4)$$

The anomaly from each lamina segment is then

$$C + \int_{\phi_1}^{\phi_2} \left(1 - \frac{Z_0}{r_n}\right) d\phi$$

where this integral is computed exactly.

It has been found, by using direct numerical integration, that for most contours the accuracy of using an approximation at only five points is better than 0.5%. However, if the field point is above and near a contour ($A_n \to 0$) or if an edge is extremely skewed ($\phi \to 0$), these errors become significant. Fortunately, in the case in which A_n is small enough to affect these errors, the difference between the curved and the flat values is less than 1% w[illegible] the approximation errors are of the order of 50% and is less t[illegible] 0.1% when the errors are as high as 100%. Thus the net result is an effective error of less than 0.5%. Also, as $\phi \to 0$, the effective area and hence the gravitational contribution approach 0, and so this source of error also becomes negligible.

The testing was done for a contour 300 km long. In practice, contours which the field points will be near are generally much shorter than this value, the errors thus being reduced to the accuracy of the machine. One could use seven or 10 points instead of five in the parabolic approximation, at small additions of time, but exhaustive testing has shown this to be unwarranted.

Acknowledgments. A large number of dedicated people are responsible for the ability to obtain information on the gravity field of the moon. Our thanks go to all of them. We particularly appreciate the computer-programming and data-processing assistance of E. L. Barnett, H. L. Moore, and S. M. Kindall at the TRW Systems Group in Houston, Texas; R. K. Osburn at the Johnson Space Center, and Leon Gove and Carolyn Dean at the Woods Hole Oceanographic Institution. We thank W. L. Sjogren for providing information in advance of publication, and we thank him and W. Bryan for review comments. This study was supported by the National Aeronautics and Space Administration at the Woods Hole Oceanographic Institution (under contract NAS 9-12563) and at the Johnson Space Center. Contribution 3528 of the Woods Hole Oceanographic Institution.

REFERENCES

Arkani-Hamed, J., On the formation of the lunar mascons, *Proc Lunar Sci. Conf. 4th*, *3*, 2673–2684, 1973.

Baldwin, R. B., *The Measure of the Moon*, 488 pp., University of Chicago Press, Chicago, Ill., 1963.

Baldwin, R. B., Lunar mascons: Another interpretation, *Science*, *162*, 1407–1408, 1968.

Baldwin, R. B., The question of isostasy on the moon, *Phys. Earth Planet. Interiors*, *4*, 167–179, 1971.

Booker, J. R., R. L. Kovach, and L. Lu, Mascons and lunar gravity, *J. Geophys. Res.*, *75*, 6558–6564, 1970.

Bryan, W. B., Wrinkle-ridges as deformed surface crust on ponded mare lava, *Proc. Lunar Sci. Conf. 4th*, *1*, 93–106, 1973.

Conel, J. E., and G. B. Holstrom, Lunar mascons: A near-surface interpretation, *Science*, *162*, 1403–1405, 1968.

De Hon, R. A., Thickness of mare material in the Tranquillitatis and Nectaris basins, paper presented at 5th Lunar Science Conference, NASA, Houston, Tex., 1974.

Hulme, G., Mascons and isostasy, *Nature*, *238*, 448–450, 1972.

Huneke, J. C., E. K. Jessberger, F. A. Podosek, and G. J. Wasserburg, $^{40}Ar/^{39}Ar$ measurements in Apollo 16 and 17 samples and the chronology of metamorphic and volcanic activity in the Taurus-Littrow region, *Proc. Lunar Sci. Conf. 4th*, *2*, 1725–1756, 1973.

Lammlein, D. R., G. V. Latham, J. Dorman, Y. Nakamura, and M. Ewing, Lunar seismicity, structure, and tectonics, *Rev. Geophys Space Phys.*, *12*, 1–21, 1974.

Marshall, C. H., Thickness and structure of the Procellarian system in the Lansberg region of the moon, *U.S. Geol. Surv. Astrogeologic Stud.*, part A, 12–18, 1963.

Muehlberger, W. R., Structural history of southeastern Mare Serenitatis and adjacent highlands, paper presented at 5th Lunar Science Conference, NASA, Houston, Tex., 1974.

Muller, P. M., and W. L. Sjogren, Mascons: Lunar mass concentrations, *Science*, *161*, 680–684, 1968.

Muller, P. M., and W. L. Sjogren, High resolution gravimetric map of the Mare Imbrium region, *Space Programs Sum. 37-54*, part 2, pp. 14–16, Jet Propul. Lab., Pasadena, Calif., 1969.

Muller, P. M., W. L. Sjogren, and W. R. Wollenhaupt, Lunar gravity: Apollo 15 Doppler radio tracking, *Moon*, *10*, 195–205, 1974.

Phillips, R. J., and R. S. Saunders, Interpretation of gravity anomalies in the irregular maria, paper presented at 5th Lunar Science Conference, NASA, Houston, Tex., 1974.

Phillips, R. J., J. E. Conel, E. A. Abbot, W. L. Sjogren, and J. B. Morton, Mascons: Progress toward a unique solution for mass distribution, *J. Geophys. Res.*, *77*, 7106–7114, 1972.

Phillips, R. J., G. F. Adams, W. E. Brown, Jr., R. E. Eggleton, P. L. Jackson, R. Jordan, W. J. Peeples, L. J. Porcello, G. G. Schaber, W. R. Sill, T. W. Thompson, S. H. Ward, and J. S. Zelenka, The Apollo 17 lunar sounder experiment: A progress report, paper presented at 5th Lunar Science Conference, NASA, Houston, Tex., 1974.

Sjogren, W. L., P. Gottlieb, P. M. Muller, and W. R. Wollenhaupt, S-band transponder experiment, *NASA Spec. Publ. SP-289*, 1972.

Sjogren, W. L., R. N. Wimberly, and W. R. Wollenhaupt, Lunar gravity: Apollo 17, *Moon*, *11*, 41–52, 1974.

Stipe, J. G., Iron meteorites as mascons, *Science*, *162*, 1402–1403, 1968.

Talwani, M., and M. Ewing, Rapid computation of gravitational attraction of three-dimensional bodies of arbitrary size, *Geophysics*, *25*, 203–225, 1960.

Talwani, M., G. Thompson, B. Dent, H.-G. Kahle, and S. Buck, Traverse gravimeter experiment, *NASA Spec. Publ. SP-330*, 1973.

Urey, H. C., Mascons and the history of the moon, *Science*, *162*, 1408–1410, 1968.

Wise, D. U., and M. T. Yates, Mascons as structural relief on a lunar 'Moho,' *J. Geophys. Res.*, *75*, 261–268, 1970.

Wood, J. A., Petrology of the lunar soil and geophysical implications, *J. Geophys. Res.*, *75*, 6497–6513, 1970.

(Received July 1, 1974;
revised July 22, 1975;
accepted August 18, 1975.)

Proc. Lunar Sci. Conf. 6th (1975), p. 2797–2804.
Printed in the United States of America

Negative gravity anomalies on the moon

CARL BOWIN

Woods Hole Oceanographic Institution,* Woods Hole, Massachusetts 02543

Abstract—Negative gravity anomalies on the moon can be categorized by whether they show a correspondence to lunar topography or appear to be unrelated to surface topography. Clear examples of the former are the negative anomalies from Doppler residual data that occur over craters such as Copernicus, Hipparchus, Ptolemaeus, Theophilus, and Langrenus. These anomalies appear to be due to mass deficiencies caused by the cratering process, in large part probably by ejection of material from the crater. Some anomalies on the far side determined from an analysis of orbital rates (Ferrari, 1975) may have a correspondence with topography, but others do not. Irregularities in the thickness of the lunar crust, not related to compensation for present surface topography, are inferred to be a likely source for the broad large gravity anomalies unrelated to surface topography. Localized large negative anomalies adjacent to mascons, such as these between Mare Serenitatis and Mare Imbrium or Mare Crisium, may be the result of localized depression of lunar crust adjacent to mare basins during the early stages of mare filling. Structures on the moon having a half-wavelength of 800 km or less, and large negative or positive gravity anomalies are not in isostatic equilibrium. Many of these features have mass loadings of about 1000 kg/cm^3 which can be statically sustained on the moon, even though such isostatic mass anomalies cannot be so maintained on the earth.

INTRODUCTION

ALTHOUGH THE LARGE POSITIVE lunar gravity anomalies (mascons) have attracted the most attention, negative gravity anomalies (free-air anomalies) have been recognized for the lunar surface since the first analysis of the gravity field of the moon (Muller and Sjogren, 1968) based on Lunar Orbiter data. The first free-air gravity anomaly map of the lunar front side, presented by Muller and Sjogren (1968), revealed minimum negative gravity anomalies of −100 mgal northwest of Ptolemaeus, two lows of −80 mgal between Mare Serentitatis and Mare Nectaris, a low of −70 mgal north of Serenitatis, two lows of −60 mgal due west of Ptolemaeus, a low of −60 mgal northwest of Mare Imbrium, and several lows of lesser magnitude. The mascons shown on the same map are +60 mgal for Mare Humorum, +100 mgal for Nectaris and Crisium, +180 mgal for Serenitatis, and +230 mgal for Imbrium. Two highs of +70 mgal apparently unrelated to circular maria were also identified, one southeast of Eratosthenes and the other farther southeast, but northwest of Sinus Medii. The closest approach of the Lunar Orbiter missions to the lunar surface was 100 km, and the anomalies were normalized to an altitude of 100 km under the assumption that mass variations were located at a depth of 50 km below the surface. Information from the Apollo missions has confirmed the existence of mascons, and led to revision of some of the other features. The only clear relationship of the orbiter gravity anomalies to

*Contribution No. 3548 of the Woods Hole Oceanographic Institution.

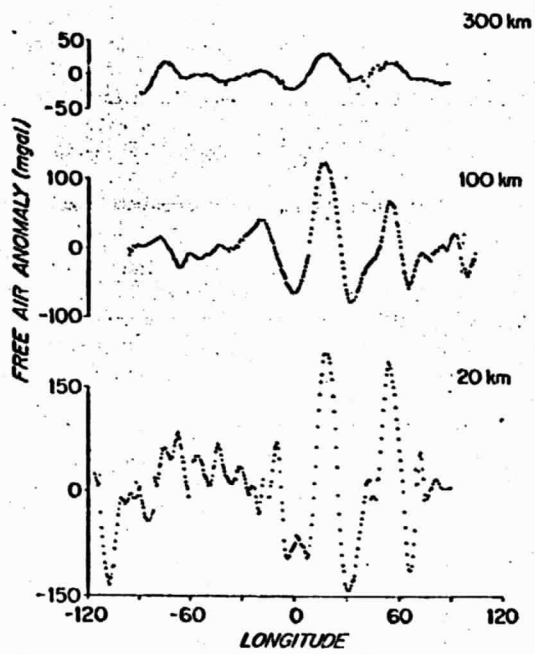

Fig. 1. Free-air gravity anomalies from Apollos 15 and 17. Profiles of total acceleration (estimate of free-air anomaly) obtained by processing Doppler data using extended sequential estimation techniques by W. Wollenhaupt at Johnson Spacecraft Center. These profiles are presented to show the attenuation of the negative anomalies with increasing height. Profile at 300-km height from Apollo 15 Rev. 1, at 100-km height from Apollo 15 Rev. 19, and at 20-km height from Apollo 17 Rev. 3.

topography is the anomalous association of the mascon anomalies with depressions in the surface at the circular maria. It was not until the later Apollo missions that gravity anomalies were determined from orbits which approached to within about 15 km of the surface. In some of those revolutions of the Apollo command ship module (CSM), negative gravity anomalies were observed to correlate with the locations of craters having diameters of less than 100 km. Thus, both gravity anomalies that correlate with topography, either directly or inversely, and those that do not are present on the moon.

High-resolution, global coverage of the lunar gravity field is not yet available. Interpretation rests upon the extremely limited surface measurements, the incomplete coverage of the moon's near side by high- and moderate-resolution gravity data obtained from analysis of Doppler residuals for individual spacecraft orbits (e.g. Fig. 1), and the lower resolution, more complete global coverage (Fig. 2) obtained from analysis of orbital rates (Ferrari, 1974, 1975). A similar global analysis also has been prepared by Ananda (1975).

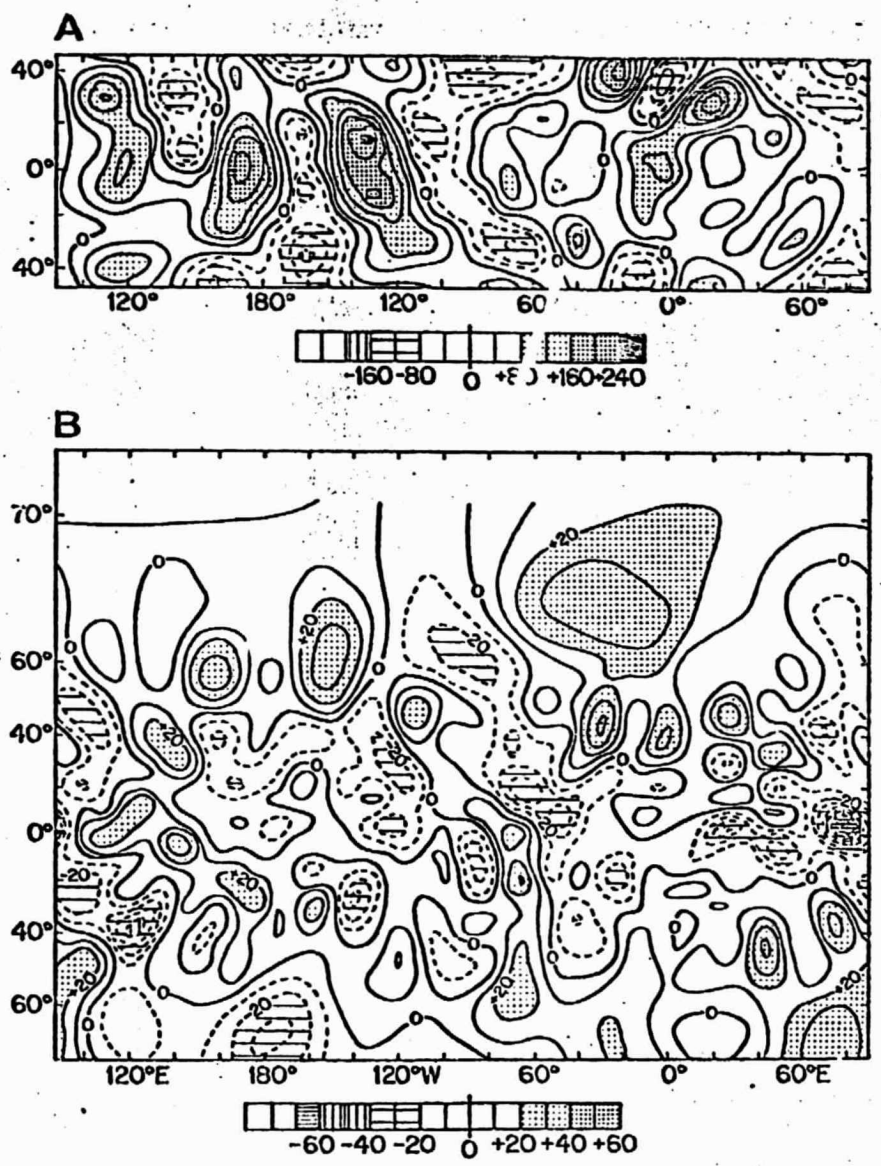

Fig. 2. Regional free-air gravity anomalies of the moon and earth. A is a fifteenth order and degree spherical harmonic free-air anomaly map at 100-km height of the lunar surface from Ferrari (1975). B is a regional free-air anomaly map of the earth at the surface from Smithsonian Astrophysical Observatory (SAO) Standard Earth II spherical harmonic coefficients referenced to the International Gravity Formula 1930: approximately a sixteenth order and degree map. Contours in milligals.

NEGATIVE ANOMALIES RELATED TO TOPOGRAPHY

Negative anomalies over unfilled craters have been observed in the gravity data obtained from tracking the low-altitude periapsis (less than 50 km) orbits of Apollo missions. These generally occurred during the early revolutions (revs.) of the Apollo missions (e.g. Fig. 1; 20-km height), prior to separation of the LEM, and more continuously in the case of the subsatellites of the Apollo 15 and 16 missions. Examples are the −57-mgal anomaly determined at about 20-km altitude above the edge of Copernicus Crater (Sjogren *et al.*, 1973, 1974), −67 mgal at about 16-km altitude nearly above the center of Hipparchus (Sjorgen *et al.*, 1972), −98-mgal anomaly determined at about 30-km altitude nearly over the center of Ptolemaeus (Sjogren, 1974), −120 mgal at about 16 km over the center of Theophilus (Sjogren *et al.*, 1972), and the −127-mgal anomaly determined at about 25 km above the edge of Langrenus (Sjogren, 1974).

These anomalies appear to be clearly due to mass deficiencies caused by the cratering process, in large part probably by ejection of material from the crater. Disk-shaped models representing the deficiency of crater depressions have been successful in reproducing the general magnitude of the observed gravity anomalies (Sjogren *et al.*, 1972; Scott, 1974). Sjogren *et al.* (1974) found that their best fit to the magnitude and gradient of the Copernicus anomaly was obtained when disk masses were included to simulate the mass of the crater rim beneath the orbit trajectory.

Negative anomalies of much broader extent than typical individual craters are common on the moon, both on the near side and on the far side (Fig. 2A). Those on the near side show little or no correspondence with topographic depressions. Some of those on the far side have been inferred by Ferrari (1974, 1975) to be associated with ringed basins such as Mendeleev, Moscoviense, Korolov, and Apollo, and he associates other ringed basins such as Hertzsprung, Ingenii, Gagarin, and Tsiolkovsky with relative lows in regions of gravity highs. The correlation of Korolov with a −110-mgal minimum and that of Apollo with a −166-mgal minimum are the best. However, the size of the ringed basins as presently known; the lack of similar anomalies over other ringed basins such as Leibnitz and Milne; the apparent lack of ringed-basin structures correlative with the −112-mgal (15N, 255E), −93-mgal (15N, 200E), −130-mgal (45S, 165E), and −145-mgal (45N, 195E) minima; and the different local gravity relief for similar sized features such as Mendeleev, Gagarin and Ingenii, and Hertzsprung and Apollo suggest that the broad negative anomalies of the back side, also, are not simply a result of topographic depressions. More refined processing of the orbital rate data may contribute to more definitive knowledge of the location and magnitude of the regional gravity anomalies.

NEGATIVE ANOMALIES NOT RELATED TO TOPOGRAPHY

The cause of these negative gravity anomalies is not obvious. They do not appear to be related to topographic depressions, and commonly occur over

highland topography. The most prominent negative anomalies encountered in the Doppler residual acceleration data are those between the Mare Imbrium and Mare Serenitatis mascon anomalies, and between the Mare Serenitatis and Mare Crisium mascons (Fig. 1). Respectively, these anomalies are about −20 and −5 mgal at 300-km height, about −80 and −60 mgal at 100-km height, and about −250 and −225 mgal at 20-km height (Siogren *et al.*, 1974; Bowin *et al.*, in press; Muller *et al.*, 1974). Figure 1 shows a sampling of the Doppler residual data for those heights but do not necessarily show the most pronounced values attained. Bowin *et al.* (in press) demonstrated that the gravity low to the east of Mare Serenitatis does not continue along the southern margin of the basin. Thus these negative anomalies apparently do not form a ring around Mare Serenitatis and very probably neither do they ring the other circular mare basins. Furthermore, they are too negative to be the result of an edge effect from a deep mass deficiency that might result if a root of crustal material existed beneath the mare basins to provide isostatic compensation, as suggested by Hulme (1972). Instead of a crustal root, a mantle dome appears to be more likely beneath the mascons. The more recent proposals for the description of mascons have been thick mare fillings (Phillips *et al.*, 1972), mantle plugs (Wise and Yates, 1970), and a combination of mantle dome and thin mare filling (Bowin *et al.*, in press). The combination explanation appears to best fit the existing gravity and geologic information. The mascons require a mass distribution that cannot be in isostatic equilibrium, and hence they indicate a strong lunar crust.

Possible explanations for the negative (and positive) gravity anomalies that are not associated with surface topography could be (1) lateral variations in crustal density, (2) lateral variations in the density of the lunar mantle, or (3) irregularities in the thickness of the lunar crust not related to compensation for surface topography. Although conceivable, lateral density variations of the magnitude required to account for the broad, large negative gravity anomalies (or positive anomalies not associated with circular maria) are not considered as likely as irregularities in the thickness of the lunar crust.

The cause of the suggested uncompensated irregularities in the thickness of lunar crust is speculative. Roughly, about 1-km variation of surface height, if uncompensated, would produce a free-air gravity anomaly variation of about 120 mgal. Assuming a lunar crust–mantle density contrast of 0.5 g/cm^3, then about 5.8 km of subcrustal variation in depth to mantle would produce about the same gravity anomaly. Erosion of a kilometer or two of surface material, as the result of impacts when the crust was rigid enough to resist isostatic adjustments of the affected areas, could possibly produce some of the observed negative gravity anomalies. If we imagine that such erosion and attendant redeposition might tend to smooth overall the lunar topography, then the gravitational contribution of the subcrustal depth variations might become evident in the external field, and produce some of the broad anomalies observed. Both negative and positive regional gravity anomalies that would not correlate with surface topography could be produced in this manner.

To explain the large negative anomalies adjacent to mare basins, (Fig. 1), the

following scenario is offered. An impact created a mare basin, beneath which a mantle dome rose to provide isostatic compensation for the deficiency of the basin above. It is also inferred that the highland rim surrounding the basin may have been higher than it is today, and that it was isostatically compensated by a crustal root into the mantle beneath. The root was probably deeper in some places than in others around the periphery of the mare basin, and these places may be the sites from which more mantle material flowed during the rise of the mantle dome. It is possible that these places have greater crustal thickness because more ejected material was deposited there. Evidence from crater counts and radioactive age dating of returned samples suggests that considerable time (perhaps about 200×10^6 yr) elapsed between the formation of the large mare basins and their filling with mare basalts (Baldwin, 1963, 1971; Huneke *et al.*, 1973). During this time interval, the rigidity of the lunar crust is inferred to have increased (Phillips *et al.*, 1972; Baldwin, 1971; Muehlberger, 1974). The initial outpourings of mare fill, which has a density about 0.5 g/cm^3 greater than that of lunar crust (Bowin *et al.*, in press; Talwani *et al.*, 1973), may have been compensated by subsidence of the mare basin. Since to a first approximation the mantle dome has the same density as the mare fill, it would not rise further to provide isostatic compensation for the subsidence of the basin floor due to the loading of the fill. The top of the dome would sink the same amount as did the basin floor. Faults at the edge of the mare fill could have isolated the adjacent crust from the subsidence taking place within the basin. However, as the rigidity of the lunar crust increased, local isostatic compensation could no longer be complete, and further subsidence of the basin, due to additional filling, would begin to depress portions of the crust surrounding the basin. Continued faulting at other portions of the basin margin may have kept their adjacent rims from being depressed. The inner edges of the shelf areas of mare basins may indicate the location of some of the sites of such concentric faulting that occurred during mare filling. Perhaps the thickness of the crust beneath the rim partially determined the degree to which different portions of the rim were depressed. Depression of crust that formerly was in isostatic equilibrium, of course, produces a mass deficiency and hence negative gravity anomalies. The more localized the area of depression, the greater will be the gravity gradients, and the greater the depression, the greater the negative anomalies. Eventually, the lunar crust became rigid enough that it could support the last fill without subsidence of the basin occurring, and, thus the excess mass of the fill together with the mass of the mantle dome produces the mascon gravity anomalies.

ISOSTASY

Kaula (1969) argued that the moon is closer to hydrostatic equilibrium than the earth because the lower degrees of the power spectrum of the lunar gravity field have lower absolute magnitude than that predicted from the earth's gravity field under the equal-stress assumption, and because the excess mass of the largest lunar mascon is smaller than that of a score of large positive anomalies on the

earth. Although the power in the low degrees is lower for the moon than for the earth, the power in the higher degrees (7–13) was determined to be higher for the moon. This relation for the higher degrees was taken by Kaula (1969) to be a consequence of errors and distortion in the analysis of the data. Figure 2, however, suggests that that relation is largely real and hence has physical significance. It is of course now desirable that the power spectrum be redetermined utilizing more recent data. O'Keefe (1968) calculated Bouguer anomalies for the lunar near side and concluded that, to a rough first approximation, the moon is in isostatic equilibrium. Baldwin (1971) seems to argue that the moon is nearly in isostatic equilibrium, including the mascons, because it approaches the condition of isostatic equilibrium as closely as the threshold strength of the lunar materials permits.

Figure 2A and the power spectrum data presented by Kaula (1969; Table 3) suggest, I claim, that structures on the moon having half-wavelengths of approximately 800 km or less are commonly not in isostatic equilibrium. These features of the gravity field represent mass loadings or deficiencies approaching about 1000 kg/cm^2, which appear to be statically maintained by the strength of the outer part of the moon. Obviously, the lower the gravitational attraction a planetary body has, the greater a mass per unit area loading it can sustain for material with equivalent strength. Thus, isostatic mass anomalies of 1000 kg/cm^2 can be statically sustained by earth-like materials on the moon, or Phobos, or Icarus, for example, but not on a body with the gravitational attraction of the sun where statically maintained isostatic anomalies of only a few kilograms per square centimeter would be expected. Neither, apparently, can so large a load be sustained on the earth. The largest isostatic mass anomalies on the earth appear to be about 1000 kg/cm^2 (Hess, 1955) and are associated with island arcs. The gravity anomalies associated with these features are not statically maintained but apparently decay rapidly upon cessation of the dynamic conditions that produce the island arcs and adjacent deep sea trenches. Furthermore, the half-wavelength of arc-trench structures is only about 200 km at the maximum.

The lunar gravity anomalies shown in Fig. 2A are much greater in magnitude than earth anomalies averaged over equivalent spacial dimensions. The fifteenth order and degree lunar anomaly map (Fig. 2A) has local gravity relief commonly of over 300 mgal. Fifteenth order on the moon is approximately equivalent to a three degree square average on the earth. In the Caribbean region, which has perhaps the greatest local gravity anomaly relief on the earth, only a little over 100-mgal relief is attained in a three degree square average (Bowin, in press).

I conclude that many structures on the moon having a half-wavelength of 800 km or less are not in isostatic equilibrium, and that mass loadings of about 1000 kg/cm^2 cannot be sustained statically on the earth as they are on the moon.

Acknowledgments—I thank W. R. Wollenhaupt for providing processed Doppler residual data for several of the Apollo missions, and he and W. L. Sjogren for many discussions regarding the lunar gravity field and its determination. A. J. Ferrari kindly provided his lunar gravity maps prior to their publication. P. Jezek and W. L. Sjogren suggested manuscript improvements. This study was supported by the National Aeronautics and Space Administration under contract NAS 9-12563.

REFERENCES

Ananda M. (1975) Farside lunar gravity from a mass point model. *Proc. Lunar Sci. Conf. 6th.* This volume.

Baldwin R. B. (1963) *The Measure of the Moon.* University Chicago Press, Chicago. 488 pp.

Baldwin R. B. (1971) The question of isostasy on the moon. *Phys. Earth Planet. Inter.* 4, 167–179.

Bowin C. *The Caribbean: gravity field and plate tectonics.* Geol. Soc. Amer. Special Paper 169. In press.

Bowin C., Simon B., and Wollenhaupt W. R., Mascons: A two body solution. *J. Geophys. Res.* In press.

Ferrari A. J. (1974) A global lunar gravity model (abstract). *EOS (Trans. Amer. Geophys. Union)* 56, 1141.

Ferrari A. J. (1975) Comparison of near and farside lunar gravity (abstract). In *Lunar Science VI*, p. 260–262. The Lunar Science Institute, Houston.

Hess H. H. (1955) The oceanic crust. *Sears Foundation: J. Mar. Res.* 14, 423–439.

Hulme G. (1972) Mascons and isostasy. *Nature* 238, 448–450.

Huneke J. C., Jessberger E. K., Podosek F. A., and Wasserburg G. J. (1973) $^{40}Ar/^{39}Ar$ measurement in Apollo 16 and 17 samples and the chronology of metamorphic and volcanic activity in the Taurus-Littrow region. *Proc. Lunar Sci. Conf. 4th*, p. 1725–1756.

Kaula W. M. (1969) The gravitational field of the Moon. *Science* 166, 1581–1588.

Muehlberger W. R. (1974) Structural history of southeastern Mare Serenitatis and adjacent highlands. *Proc. Lunar Sci. Conf. 5th*, p. 101–110.

Muller P. M. and Sjogren W. L. (1968) Mascons: lunar mass concentrations. *Science* 161, 580–684.

Muller P. M., Sjogren W. L., and Wollenhaupt W. R. (1974) Lunar gravity: Apollo 15 Doppler radio tracking. *The Moon* 10, 195–205.

O'Keefe J. A. (1968) Isostasy on the Moon. *Science* 162, 1405–1406.

Phillips R. J., Conel J. E., Abbot E. A., Sjogren W. L., and Morton J. B. (1972) Mascons: Progress toward a unique solution for mass distribution. *J. Geophys. Res.* 77, 7106–7114.

Scott D. H. (1974) The geologic significance of some lunar gravity anomalies. *Proc. Lunar Sci. Conf. 5th*, p. 3025–3036.

Sjogren W. L. (1974) Lunar gravity: Apollo 16. *The Moon* 11, 35–40.

Sjogren W. L., Gottlieb P., and Muller P. M. (1972) Lunar gravity via Apollo 14 Doppler radio tracking. *Science* 175, 165–168.

Sjogren W. L., Wollenhaupt W. R., and Wimberly R. N. (1973) S-Band transponder experiment. In *Apollo 17 Preliminary Sci. Report*, NASA publication SP-330, p. 14-1 to 14-4.

Sjogren W. L., Wimberly R. N., and Wollenhaupt W. R. (1974) Lunar gravity: Apollo 17. *The Moon* 11, 41–52.

Talwani M., Thompson G., Dent B., Kahle H.-G., and Buck S. (1973) Traverse gravimeter experiment. In *Apollo 17 Preliminary Sci. Report*, NASA publication SP-330, p. 13-1 to 13-13.

Wise D. U. and Yates M. T. (1970) Mascons as structural relief on a lunar 'Moho'. *J. Geophys. Res.* 75, 261–268.

ABSTRACT FORM

INSTRUCTIONS FOR PREPARATION OF ABSTRACT TO BE REDUCED AND REPRODUCED BY PHOTO-OFFSET PROCESS: Type Single Space (Pica preferred) within margins only. Indent 10 spaces on first line and begin with the TITLE IN CAPS; follow with Author(s) and Affiliation, e.g., D. J. Jones, Geophysics Corp. of America, Bedford, Mass., 01730 (abbreviate where appropriate). Start Abstract on new line, indent 5 spaces. Mail Abstract to ABSTRACTS, The Lunar Science Institute, 3303 NASA Road 1, Houston, Texas 77058.

COMPARISON OF GRAVITY ANOMALIES FOR EARTH, MARS, AND MOON

Carl Bowin, Woods Hole Oceanographic Institution
Woods Hole, Massachusetts 02543

It is only within the last eight years that man has been able to compare gravity anomalies with topography on planetary bodies other than his own. Topography shows the distribution of surface irregularities, and gravity anomalies show the distribution of mass anomalies. The coherence, or lack of it, between these two parameters provides significant information on crustal structure and its evolution.

On the earth at small scales (less than 100 to 300 km half wavelength) there is generally a positive correlation between free-air gravity anomalies and topography. However, towards the larger dimensioned features, the free-air anomalies are commonly reduced in amplitude indicating partial to complete compensation for the mass of the topography. From gravity anomalies and topography the thickness of the elastic part of the lithosphere may be estimated (1). These studies suggest a thickness for oceanic lithosphere of about 10 km near spreading ridges, to values near 30 km for 60 million year old lithosphere to about 41 km in older lithosphere at deep sea trenches. Beneath continents the elastic part of the lithosphere may be about 60 km thick (2). Mass loadings of up to about 400 kg/cm^2 can be statically maintained on the earth as with the example of the Ninety East Ridge in the Indian Ocean (3). The greatest mass anomalies are associated with trenches where mass deficiencies approaching 1,000 kg/cm^2 occur (4). As pointed out previously (5), the gravity anomalies associated with trenches are not statically maintained, but decay rapidly upon cessation of the dynamic conditions that produce island arcs and adjacent deep sea trenches. On the earth, the largest gravity anomalies are associated with features that have half wavelengths of less than 200 km and that are dynamically maintained by the plate tectonic processes active today.

At large scales (greater than 100 to 300 km half wavelength) there is generally a lack of coherence between free-air gravity anomalies and topography, and the anomalies over the vast majority of the surface are small in magnitude (less than 30 mgal for spherical harmonic models of degree and order 16)(6), indicating rather close adjustment to isostatic equilibrium.

Mars has a radius of only about half that of the earth, and a surface gravitational attraction only 38% as great. However, Mars has very large regional gravity anomalies. Mariner 9 Doppler data provides information on the gravity field variations to the resolution of an eight or nine degree and order model (7, 8, 9, 10). Measured free-air anomalies range from -300 mgal to +500 mgal (11). The large martian gravity anomalies correlate well with regional topographic variations, the high positive values occurring over the Tharsis Plateau region, and the negative values over the Chryse and amazonis lowlands. The anomalies, however, are only about four-tenths as great as they would be if the topography were not partially compensated (11). The remainder of the martian topography, at least at the resolution of 8th order, is considerably nearer to being in isostatic compensation, although anomalies 50 to 100 mgal from zero are common. The isostatic deviation map prepared by

Phillips and Saunders (11) indicates a 1,200 kg/cm^2 mass anomaly associated with the Tharsis Plateau region. The mass anomalies associated with the giant shield volcanoes are not yet resolvable.

The moon's gravity anomalies indicate that structures having half-wavelengths of approximately 800 km or less are commonly not in isostatic equilibrium (5). Globally its gravity anomalies have been determined to a spherical harmonic model representation of fifteenth order and degree (12). Free-air gravity anomalies at 100 km altitude range from -166 to +260 mgal. Both these extremes are located on the lunar farside where control is the weakest. The range of frontside anomalies is from -137 to +239 mgal. At 100 km altitude, a fifteenth order model for the earth shows a range of free-air anomalies from -0.1 to +0.1 mgal. On the lunar nearside the large positive anomalies are all associated with mascons and indicate mass anomalies of about 800 kg/cm^2 (13,14).

The available data for three planetary bodies indicates the following comparison. The magnitude of the maximum gravity anomalies and the mass per unit area anomalies differ by less than a factor of two amongst the three bodies. The areal size of the maximum anomalies, however, differ much more markedly. On the earth they are restricted to half wavelengths of less than 200 km. On the moon they extend up to half wavelengths of 800 km. But on Mars they extend to over a 4,000 km half wavelength! On the earth, the largest gravity anomalies require dynamic processes to maintain them. Maximum static loads that can be sustained appear to be on the order of 500 kg/cm^2, and this low value is presumably due to the thinness of the rigid lithosphere. For the earth and Mars, the large gravity anomalies generally are correlated with topography. The mascons on the moon, however, are inversely correlated with topography, the large positive anomalies occurring over mare basins on the nearside. The large anomalies determined for the farside have been inferred to be positively correlated with regional topography irregularities (12) but this generality has been questioned (5). Visual inspection of the topographic and gravity Lunar Orbital Data Maps recently published (13, 14), allowing for the different resolutions, does not support a strong correlation of topography and gravity on the farside. The planned Lunar Polar Orbiter mission should resolve the matter. Each of the three bodies appears to have experienced a period during which its crust was largely in isostatic equilibrium. The moon left this stage about 3 b.y. (17), Mars developed the Tharsis Plateau perhaps within the last 1 b.y. (11, 18), and the earth's crust remains preponderantly in isostatic equilibrium. Although the mascon mass anomalies lie within 100 km of the lunar surface (13,14), it is no doubt a thick rigid lithosphere that supports them. Although the Tharsis mass anomaly on Mars is greater than the lunar mascons, this does not necessarily require a thicker rigid lithosphere on Mars. It seems more likely that on the moon there was simply not sufficient extrusion of dense volcanic material to create larger mascons.

The gravity data is compatible with the moon, Mars, and the earth being examples of an evolutionary sequence. The moon became frozen at the youngest age, perhaps while bombardment was still at a moderately high flux. Mars developed greater volcanic activity, supplying greater volume to the outer part of the crust than did the moon, following development of a thick lithosphere. The Tharsis Plateau region may be a gigantic lacolith. The shield volcanoes

of Mars may be terminal volcanic outbursts. The earth's heat engine appears to have had the greatest sustaining power and plate tectonic activity developed, and a thin lithosphere persists.

Perhaps Mars offers a clue to the origin of the asteroid belt. I suggest that a planetary body that formerly existed there, in evolving through the volcanic stage developed a surficial mass anomaly significantly larger than that observed in the Tharsis Plateau. Sjogren et al. (7) found that a single anomalous mass about 0.8×10^{-3} M_{Mars} located beneath the Tharsis region at a radial distance of 0.571 R_{Mars} accounted for the main features of the anomalous gravity field. We may take this as a reasonable estimate of the mass of the Tharsis Plateau anomaly, but its actual depth would be much shallower because of its broad spacial dimensions. A larger mass anomaly in the outer portion of a planetary body might lead to instabilities of its motion causing its break-up.

REFERENCES

1. McKenzie, D.P., and C.O. Bowin (in press). Watts, A.B., J.R. Cochran and G. Selzer (1975) J. Geophys. Res., 80, 1391-1398. Watts, A.B., and J.R. Cochran (1974) Geophys. J. Roy. Astr. Soc., 38, 119-141. LePichon, X., J. Francheteau and J. Bonnin (1973) Plate Tectonics, Elsevier, Amsterdam, 300 p.
2. Walcott, R.I. (1970) J. Geophys. Res., 75, 3941-3954.
3. Bowin, C.O. (1973) J. Geophys. Res., 78, 6029-6043.
4. Hess, H.H. (1955) J. Marine Res., 14, 423-439.
5. Bowin, C.O. (1975) Proc. Lunar Sci. Conf. 6th, 3, 2797-2804.
6. Lerch, F.J., C.A. Wagner, J.A. Richardson, and J.E. Brownd (1974) Ref. No. X-921-74-145, Goddard Space Flight Center, 100 p.
7. Sjogren, W.L., J. Lorell, L. Wong, and W. Downs (1975) J. Geophys. Res., 80, 2899-2908.
8. Reasenberg, R.D., I.I. Shapiro, and R.D. White (1975) Geophys. Res. Letts. 2, 89-92.
9. Born, G.H. (1974) J. Geophys. Res., 79, 4837-4844.
10. Lorell, J., G.H. Born, E.J. Christensen, P.B. Esposito, J.F. Jordan, P.H. Laing, W.L. Sjogren, S.K. Wong, R.D. Reasenberg, I.I. Shapiro, and G.L. Slater (1973) Icarus, 18, 304-311.
11. Phillips, R.J. and R.S. Saunders (1975) J. Geophys. Res., 80, 2393-2398.
12. Ferrari, A.J. (1975) Science, 188, 1297-1300.
13. Phillips, R.J., J.E. Conel, E.A. Abbot, W.L. Sjogren and J.B. Morton (1972) J. Geophys. Res., 77, 7106-7114.
14. Bowin, C.O., B. Simon, and W.R. Wollenhaupt (1975) J. Geophys. Res., 80, 4947-4955.
15. Bills, B.G. and A.J. Ferrari (1975), Proc. Lunar Sci. Conf. 6th, 3, Lunar Orbital Data Map.
16. Ananda, M.P. and A.J. Ferrari (1975), Proc. Lunar Sci. Conf., 6th, 3, Lunar Orbital Data Map.
17. Husain, L. (1974) J. Geophys. Res., 79, 2588-2606.
18. Mutch, T.A. and J.W. Head (1975) Rev. Geophys. Space Phys., 13, 411-416.